Cerebral Cortex May 2010;20:1187–1194
doi:10.1093/cercor/bhp182
Advance Access publication September 3, 2009

Noninvasive Functional and Structural Connectivity Mapping of the Human Thalamocortical System

Dongyang Zhang[1], Abraham Z. Snyder[1], Joshua S. Shimony[1], Michael D. Fox[1] and Marcus E. Raichle[1,2,3,4,5]

[1]Department of Radiology, [2]Department of Neurology, [3]Department of Neurobiology, [4]Department of Psychology and [5]Department of Biomedical Engineering, Washington University, St Louis, MO 63110, USA

Relating structural connectivity with functional activity is fundamentally important to understanding the brain's physiology. The thalamocortical system serves as a good model system for exploring structure/function relationships because of its well-documented anatomical connectivity. Here we performed functional and structural magnetic resonance mapping of the human thalamocortical system using intrinsic brain activity and diffusion-weighted imaging. The accuracy of these imaging techniques is tested by comparison with human histology registered to common anatomical space and connectional anatomy derived from non-human primates. In general, there is good overall concordance among structural, functional, and histological results which suggests that a simple model of direct anatomical connectivity between the cerebral cortex and the thalamus is capable of explaining much of the observed correlations in neuronal activity. However, important differences between structural and functional mapping results are also manifest which suggests a more complex interpretation and emphasizes the unique contributions from structural and functional mapping.

Keywords: DTI, fcMRI, functional connectivity, resting state, thalamus

Introduction

The functional repertoire of any system is ultimately determined by its structural composition. Equally important in the brain, the underlying structure is continually reshaped by function in relation to experience. This interdependence underscores the importance of exploring the relationship between structure and function in neuroscience. Cellular electrophysiology provides a window on function but only with sparse sampling. Likewise, invasive tract tracing, especially performed postmortem, is similarly limited in its areal coverage. Recent developments have enabled whole brain characterization of both neuronal activity using functional magnetic resonance imaging (fMRI) and large fiber tracts using diffusion tensor imaging (DTI). The combination of these two imaging modalities permits a systems level interrogation of functional interactions and their structural underpinnings. However, most of the existing dual imaging studies are limited in the scope of their functional measures by reliance on task performance to elicit measurable neuronal activity (Toosy et al. 2004; Baird et al. 2005) (for a review of this extensive literature; see Rykhlevskaia et al. 2008). First, each task activates a very restricted set of brain regions, and second, a "wired together" interpretation of coactivations must be dissociated from the confound of stimulus driven synchrony. If the goal is a global characterization of structure/function relationships in the brain, reliance on task performance may not be the most efficient approach.

An alternative to the task-based approach to studying the brain's functional organization is to examine the organization of its ongoing functional activity. A factor motivating this approach is the fact that the majority of the brain's enormous energy budget is devoted to its ongoing functional activity rather than evoked activity (Raichle and Mintun 2006). In fact, less than 5% of its energy budget is devoted to momentary task demands (Raichle and Mintun 2006). Ongoing fluctuations in the blood oxygen level–dependent (BOLD) fMRI signal provide a unique view of the organization of intrinsic activity. The ongoing activity revealed by the fMRI BOLD signal persists across different states of consciousness including wakefulness (Biswal et al. 1995; Lowe et al. 1998; Cordes et al. 2000; Greicius et al. 2003), sleep (Horovitz et al. 2008; Larson-Prior et al. 2009), anesthesia induced unresponsiveness (Johnston et al. 2008), and coma (Boly et al. 2008). Ongoing activity exhibits correlated signaling within neuroanatomically defined systems that replicate with remarkable precision responses to experimentally administered tasks (Vincent et al. 2007). In this way, multiple functional networks can be delineated from a single scan without the need for any task performance (Fox and Raichle 2007).

The focus of the current study is to map structural and functional connections between the human thalamus and cortex. The thalamus is a core structure of the brain that contains primary relay nuclei that are highly specific in their connections with distinct zones of the cerebral cortex. A seminal study has previously investigated the structural connectivity of the human thalamocortical system using DTI and probabilistic tractography (Behrens, Johansen-Berg, et al. 2003). A specific question we were interested in was how well structural information derived from DTI compares with functional information derived from fMRI of intrinsic brain activity (Zhang et al. 2008). Furthermore, how well does structural and functional MR mapping compare with "gold standard" histological parcellation of the human thalamus and connectional anatomy inferred from non-human primates? We hypothesized that, in general, correlations in intrinsic neuronal activity should correspond well with connectional anatomy derived from DTI, but important differences may be observed given that complex neuronal interactions occur via polysynaptic pathways and given that the strength of an anatomical connection is not always reflective of the importance of its functional role (Van Horn et al. 2000; Sherman and Guillery 2006). Therefore, in considering thalamocortical "connectivity", defining a *functional* connectivity map may be just as important as defining a *structural* connectivity map of the thalamocortical system, each providing unique information relevant to the physiology of the system.

Materials and Methods

Subjects/Data Acquisition

Intrinsic brain activity was assessed with BOLD fMRI in a group of 17 subjects (3T Siemens Allegra MR scanner [Erlangen, Germany], 4-mm isotropic voxels, time echo [TE] = 25 ms, time repetition [TR] = 2.16 s, 776 frames per subject). Subjects visually fixated on a projected cross-hair. No other task was imposed except to remain still and not fall asleep. Structural fiber tracks were assessed using diffusion-weighted MRI (DWI) acquired in a group of 12 subjects using a 1.5T Siemens Sonata MR scanner. Diffusion was measured in 48 directions plus 4 unsensitized volumes (2.0- to 2.5-mm isotropic voxels, TE = 113 ms, TR = 7 s, *b* value = 400–1200 s/mm^2). Five DTI data sets were acquired in each individual. Total acquisition time was approximately 90 min per subject. All data were acquired in the course of previously published and unpublished studies (Shimony et al. 2006; Fox et al. 2007). Although structural and functional imaging were performed in two separate groups, it is unlikely that *the current study* would benefit from dual modality imaging on the same individuals due to methodological variability in imaging a small subcortical structure at the *single subject* level (see Supplemental Materials for an extended discussion). Dual modality imaging in a separate population of 3 subjects supports this assertion (data not shown). In the current results, all data presented were analyzed at the *population* level. Anatomical images acquired for definitive atlas transformation included a T_1-weighted magnetization–prepared rapid gradient echo (MP–RAGE) and a T_2-weighted (T2W) fast spin echo scan.

Cortical Regions of Interest Definition

Five cortical regions were manually drawn on the cortical surface using CARET (Van Essen 2005; Van Essen et al. 2001) (see Zhang et al. 2008) on the basis of major sulcal landmarks, largely following previous work taking into account the known anatomical connectivity of the thalamus and the cortex (Behrens, Johansen-Berg, et al. 2003; Zhang et al. 2008). These cortical regions of interest (ROIs) were defined as 1) fronto-polar and frontal cortex including the orbital surface and anterior cingulate; 2) motor and premotor cortex (Brodmann areas 6 and 4) excluding adjacent portions of cingulate cortex; 3) somatosensory cortex (Brodmann areas 3, 1, 2, 5, and parts of 40); 4) parietal and occipital cortex including posterior cingulate and lingual gyrus; 5) temporal cortex including the lateral surface, temporal pole and parahippocampal areas (Fig. 1*a*). For our functional connectivity MRI (fcMRI) study, BOLD data were first registered to our standard atlas space which ensured correct alignment with our cortical ROIs. For our DWI study, tractography was performed in native acquisition space. Therefore, our cortical ROIs were first deformed to each subject's anatomy using CARET's surface-based registration (Van Essen and Drury 1997; Van Essen et al. 2001), and then converted to volume space with an assigned cortical thickness of 3 mm (1.5 mm above and below fiducial surface corresponding to "layer IV").

Resting-State fcMRI Preprocessing and Analysis

Preprocessing included compensation for systematic, slice-dependent time shifts, elimination of systematic odd-even slice intensity differences due to interleaved acquisition, rigid body correction for head motion within and across runs, and normalization of the signal intensity across each run (skipping the first four frames) to obtain a whole brain mode value of 1000 (Ojemann et al. 1997). Atlas transformation was achieved by composition of affine transforms connecting the first functional volume (averaged over all fMRI runs after cross-run realignment) with the T2W and T_1-weighted structural images. Common mode image registration (e.g., to correct for head motion within and across fMRI runs and affine warping of T_1-weighted structural images to the atlas-representative target image) was performed using in-house versions of standard algorithms (Woods et al. 1998). Cross-modal registration (e.g., T2W to T_1-weighted images) was performed using the vector gradient measure maximization (Rowland et al. 2005). Our atlas representative template includes MP–RAGE data from 12 normal individuals and was made to conform to the 1988 Talairach atlas (Talairach and Tournoux 1988; Lancaster et al. 1995). Linear trends across runs were removed voxelwise and the data were low-passed to retain frequencies below 0.1 Hz. Several sources of spurious variance were removed by regression of the following nuisance variables along with their first derivatives: 1) the six parameters resulting from rigid body correction for head motion; 2) a signal from a ventricular region of interest; and 3) a signal from a white matter region of interest (Fox et al. 2005). To prepare our BOLD data for the present analyses, each fMRI run was resampled to 2-mm^3 voxels in atlas space.

To map correlations in intrinsic brain activity between the cortical ROIs and the thalamus, the following analysis was performed. First, the average BOLD time course was extracted from each cortical ROI. Then, the partial correlation was computed between each of these cortical ROI time course and the time course extracted from each thalamic voxel, eliminating the shared variance among all the cortical ROI time courses (Zhang et al. 2008). For purposes of calculating statistical significance, partial correlation coefficients were converted to a normal distribution using Fisher's *r*-to-*z* transform. Because consecutive BOLD frame are not independent but autocorrelated, it was necessary to

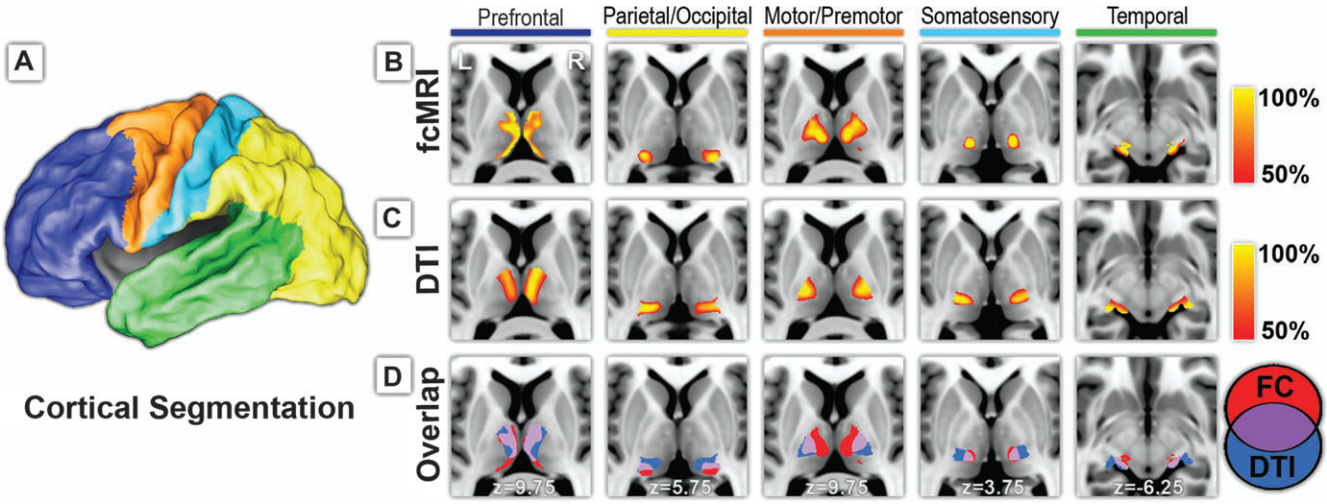

Figure 1. Structural and functional connectivity between cerebral cortex and thalamus. (*A*) The cortex is partitioned on the basis of major anatomical landmarks into 5 nonoverlapping regions using surface-based ROI definition from CARET (Van Essen 2005; Van Essen et al. 2001). (*B*) Each cortical area demonstrated specific correlations in its intrinsic neuronal activity with distinct areas of the thalamus. (*C*) Probabilistic tractography likewise demonstrated specificity of tracking white matter fiber tracks between the thalamus and each cortical area, similar to Behrens et al. (2003). (*D*) Structural and functional mapping results demonstrated considerable overlap in their connectivity profiles (purple).

correct the degrees of freedom according to Bartlett's theory (Jenkins and Watts 1968). Accordingly, for purposes of significance testing under a fixed-effects model, the z transformed partial correlation values were converted to Z scores by multiplying by $\sqrt{(n-k-3)}$, where n is the degrees of freedom (number of frames divided by 3.183) and k is the order of the partial correlation (in the present analysis $k = 4$) (Weatherburn 1949). Z score maps were combined across subjects using a fixed-effects analysis. Thresholding for displayed Figures 1 and 4 was set to half of the maximum partial correlation value for the given thalamic map. Thus, figures are labeled as 50% and 100% corresponding to half maximum and maximum partial correlation values. To reduce bias due to possible outlier values, the maximum partial correlation value was defined as the 99th percentile value instead of the 100th percentile value. Voxels displayed using a 50% threshold all pass a multiple comparisons criteria (false positive error rate of 5%) empirically determined using a bootstrap procedure (see Zhang et al. 2008 for details).

DWI Preprocessing and Analysis

Each DWI data set was assembled by collating slices from two interleaved scans. Head motion correction was performed according to the methods of referenced work (Shimony et al. 2006). All DWI computations were performed in native acquisition space thereby minimizing resampling of the data. Subsequent analysis was performed with FMRIB's Diffusion Toolbox (FDT) as part of the FSL package (FSL v4.1.2, FDT v2.0, Oxford, UK) (Behrens, Woolrich, et al. 2003; Smith et al. 2004; Behrens et al. 2007; Woolrich et al. 2009). First, eddy current correction was applied. Then, the local probability density function of a diffusion tensor model was calculated using an algorithm that models intravoxel crossing fibers (Behrens et al. 2007). Probabilistic tractography was performed at a global level starting from each voxel in the thalamus and then tracked to its ipsilateral cortex (Behrens, Johansen-Berg, et al. 2003; Behrens, Woolrich, et al. 2003). The probability of connectivity from a thalamic voxel to a cortical ROI was calculated to be the number of fiber tracts successfully propagated to a given cortical ROI divided by the total number of tracts propagated to all cortical ROIs. This last preprocessing step is not normally performed in probabilistic tractography (see Behrens et al. 2007; Behrens, Johansen-Berg, et al. 2003; Johansen-Berg et al. 2005, for examples). However, it should be noted that inclusion of this step results in higher overlap for all cortical ROI measures both in fcMRI and in DTI results (i.e., all values in Table 1). Therefore, there is methodological value to this step as well as the possibility that the *ratios* of probabilistic tractography values are, to a degree, reflected in the cofluctuation of neuronal activity.

Post-tractography intersubject spatial alignment was performed for group level analysis. The spatial relationships among diffusion volumes, atlas representative target, T_1-weighted and T2W images were computed using previously published methods (Shimony et al. 2006). Population level probability maps were calculated using a fixed effects model. The same thresholding methodology applied to functional mapping results was applied to the population level DWI results. Thus, DWI maps display values between approximately 50% and 100% of maximum calculated probability value. For display purposes, voxel boundaries for both fcMRI and DTI results were smoothed using fourfold interpolation and then displayed using in-house software written on the MATLAB platform (The MathWorks; Natick, MA). The T_1-weighted anatomical image displayed behind our MR results is the Montréal Neurological Institute's (MNI) 152 subject average registered to common space using non-linear transform and distributed with FSL (Jenkinson and Smith 2001; Smith et al. 2004; Woolrich et al. 2009). We performed affine transform to register the MNI152 template to our standard atlas target.

Table 1

For each thalamic map, percent overlap is calculated as the number of voxels that overlap between the two methods (Fig. 1*D*, purple) divided by the total number of voxels that exceed threshold (see Fig. 1*B*,*C*)

Cortical partition	Percentage of overlapping voxels	
	fcMRI map	DTI map
Prefrontal	57%	41%
Parietal/occipital	35%	41%
Motor/premotor	36%	53%
Somatosensory	73%	25%
Temporal	56%	20%

3D Reconstruction of the Human Brain using 2D Histological Slices

The *Atlas of the Human Brain in Stereotaxic Space* by Mai, Paxinos, Voxx (hereafter referred to as the "Mai atlas") provided serial coronal sections of a 24-year-old male's brain (Mai et al. 2008). In the generation of this atlas, a variety of morphometric measures and staining techniques were utilized to partition and label various subcortical as well as cortical structures. We reconstructed the 3-dimensional brain volume from these 2-dimensional histological slices using 1-dimensional interpolation with a lookup table of slice coordinates in mm units along the y-axis (implemented using MATLAB's interpolation algorithm, The Mathworks). To facilitate comparison our functional and DWI MR results with this atlas, we spatially registered all images to a common atlas representative target. Registration of functional and DWI images are described in the above respective sections. Cross modal registration of the Mai atlas with our T_1 atlas was performed using vector gradient measure maximization (Rowland et al. 2005). Spatial relationships between the source and target images were defined in terms of affine transforms.

Monte Carlo Calculation of Significance of Overlap between fcMRI and DTI Results

The simulation consisted of recreating all thalamic voxels, assigning each voxel a binary value (Fig. 1*D*). The proportion of voxels assigned a value of 1 instead of 0 is determined by the number of voxels that exceeded the 50% threshold in the MR results (Fig. 1*B*,*C*). In this way, the thalamus was simulated for both the fcMRI results and the DTI results. Overlap between fcMRI and DTI maps was calculated as the number of simulated voxels that contained a value of 1 in both maps. The simulation was repeated 10 000 times, each time randomly permuting which voxels of the thalamus were assigned a value of 1. This null distribution was then compared with the empirical number of voxels in the overlap from Figure 1*D* to calculate statistical significance. The above steps were performed 5 separate times, once for each cortical ROI.

Results

Five cortical regions shown in Figure 1*A* were defined based on major sulcal landmarks (Van Essen 2005; Van Essen et al. 2001), taking into account the anatomical connectivity between the thalamus and the cortex. For our functional study, the average BOLD signal was extracted from each cortical region and compared with the BOLD signal at each voxel in the thalamus using partial correlation to eliminate shared variance among all cortical regions (Zhang et al. 2008). Figure 1*B* demonstrates the specificity of these functional connections. Each cortical region was specifically correlated with distinct, spatially restricted zones within the thalamus. For our structural study using DTI, we adopted a parallel approach of relating the thalamus to its ipsilateral cortex using the implementation of Behrens, Johansen-Berg, et al. (2003; Behrens et al. 2007). Distinct zones of thalamic connectivity were observed for each cortical region in a distribution similar to that of Behrens, Johansen-Berg, et al. (2003) (Fig. 1*C*). The overlay between fcMRI and DTI results is shown in Figure 1*D*. Even though the physical basis of the two MR measurements is vastly different, there is significant overlap in their connectivity profiles ($P <$ .00001). Table 1 shows the percentage of thresholded voxels that overlap between the two methods. Additionally, multiple thalamic maps were condensed into a single winner-take-all

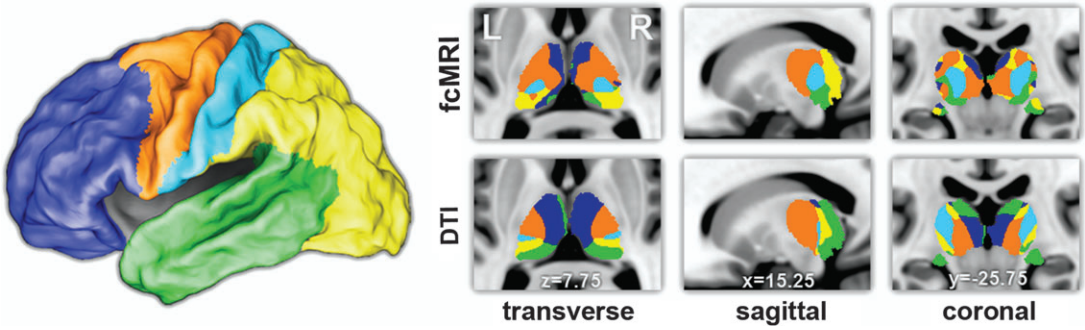

Figure 2. Winner-take-all projections of the thalamic maps presented in Figure 1. Every thalamic voxel is labeled with the color of the cortical ROI that generated the highest partial correlation or highest tractography probability values using fcMRI and probabilistic DTI, respectively.

projection (Fig. 2) in which every thalamic voxel is labeled with the color of the cortical ROI that generated the highest partial correlation or highest tractography probability value using fcMRI and probabilistic DTI, respectively.

Evaluation of Connectivity Overlap

For an evaluation of the accuracy of our imaging results compared with histology, we constructed a 3-dimensional interpolation of a coronal atlas of thalamic histology created by Mai et al. (2008). This atlas was registered to our standard anatomical space by performing cross modal matching of gyral and sulcal contours which allowed for comparisons at a voxelwise level with our MR imaging results, notwithstanding subject-to-subject variability from an atlas characteristic of a single individual. Figure 3*A* shows a representative axial slice of labeled thalamic histology. In comparing our MR results with histology, we first evaluated the localization of the overlap area between the two methods (Fig. 1*D*, purple). The overlap between motor/premotor fcMRI and DTI results traced on top of the Mai atlas (Fig. 3*B*) highlights the ventral lateral (VL) and ventral lateral posterior (VLP) thalamic nuclei, which corresponds well with documented connectional neuroanatomy (Ray and Price 1993; Jones 2007). Thalamic connectivity with other cortical regions similarly demonstrated close correspondence with neuroanatomy. The area of overlap between the two methods with prefrontal cortex localized to mediodorsal (MD) nucleus as well as ventral anterior nuclei and parts of the anterior group of thalamic nuclei (Fig. 3*C*). Overlap with temporal cortex localized well with the medial geniculate nucleus (MGN, Fig. 3*D*) and medial pulvinar (Supplemental Fig. 1). Overlap with parietal and occipital cortex localized predominantly with lateral pulvinar (Fig. 3*E*). fcMRI results also localized to the lateral geniculate nucleus (LGN), whereas DTI localization to LGN was not as pronounced (see Supplemental Fig. 1 for localization as well as a discussion of this difference). Both methods demonstrated connectivity between the somatosensory cortex and relevant parts of the thalamus. The overlap between the two methods localized predominantly to anterior pulvinar, which projects mainly to Brodmann area 5 (BA5) (Fig. 3*F*). DTI results also highlighted ventral posterior lateral (VPL) nuclei, whereas fcMRI results were localized more medially to just anterior pulvinar (Supplemental Fig. 1).

Evaluation of Connectivity Differences

The greatest difference (by total voxel count) in the present thalamic localization results was observed in the lateral extent of the MD nucleus (Fig. 4, crosshairs). Although neuronal activity in motor/premotor cortex was correlated with nuclei VL/VLP, the strongest functional correlations were observed more medially in nucleus MD (Fig. 4*A*,*C*). In contrast, MD showed highest probability of DTI connectivity with prefrontal cortex (Fig. 4*B*–*D*), which is concordant with connectional anatomy derived from invasive track tracing studies in monkeys (Jones 2007). This difference is not the consequence of the level of thresholding and changes in boundary size with different levels of thresholding because the *strongest* functional correlations occur at a locus of the thalamus that is a *transition zone* in the tractography results from high connectivity with motor/premotor to high connectivity with prefrontal cortex.

We investigated this difference from the perspective of our cortical ROIs. Because each anatomically defined cortical ROI includes extended regions of gray matter that encompass multiple functional systems, it is likely that the average signal extracted from each ROI does not uniformly correlate with all voxels within that ROI. The same partial correlation analysis that generated maps in Figure 1*B* was now extended to the cortex. Figure 4*E* shows the results of this analysis. As one can see, most of the maps show cortical correlations that are well-restricted to within the cortical ROIs that generated the map. However, the prefrontal ROI correlation map not only highlights the prefrontal cortex but clearly includes a relatively intact default mode network (DMN), the only functional network to prominently retain its long range functional connections. This is to be contrasted with prefrontal connectivity with DTI tractography which predominantly tracks to lateral and not medial prefrontal cortex (i.e., outside of the DMN) because of crossing fiber issues from the corpus callosum. Motor/premotor correlations also show hints of functional system contribution in highlighting the parietal component of the dorsal attention system, though this effect was much weaker. It should be noted that the areas of largest difference between fcMRI and DTI tractography (Fig. 4*A*,*B*) concern the prefrontal and motor/premotor cortex.

Areas of highest probability in the DTI results tend to localize near the surface of the thalamus where anisotropy is highest, whereas functional localization does not preferentially localize to the outer thalamic surface (Fig. 1*B*,*C*). No consistent systematic shifts were observed between the fcMRI and DTI results, ruling out the possibility of systematic biases due to anatomical registration. Connectivity between LGN and parietal/occipital cortex was clearly seen with fcMRI but less clear with DTI, as noted above (Supplemental Fig. 1). On the other hand,

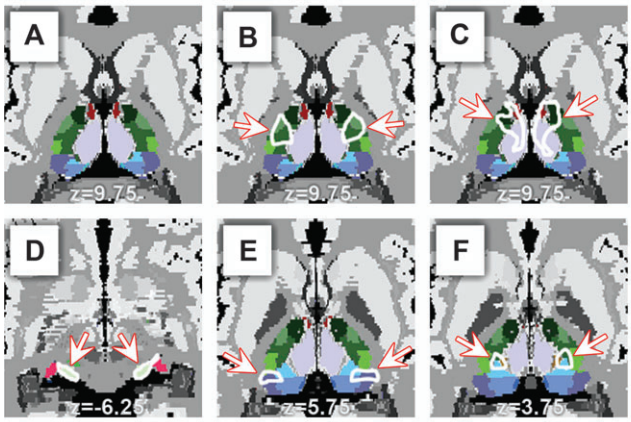

Atlas Color	Principal Cortical Target
Mediodorsal (MD)	Frontal eye field; Orbitofrontal; Lateral Frontal; Medial Frontal
Anterior group (AV; AM; AD)	Cingulate; Retrosplenial; Anterior Limbic
Ventral Anterior (VA)	Diffuse Prefrontal and Cingulate
Ventral Lateral (VL)	Mainly Premotor
Ventral Lateral Posterior (VLP)	Mainly Motor
Ventral Posterior Lateral (VPL)	SI (BA3,2,1); SII
Anterior Pulvinar	Brodmann Area 5
Lateral Pulvinar	Parietotemporal and diffuse to Occipital
Medial Pulvinar	Superior Temporal Gyrus
Lateral Geniculate Nucleus (LGN)	Striate Area
Medial Geniculate Nucleus (MGN)	Auditory Cortex (AI; AII)

Figure 3. Correspondence between structural/functional imaging and human histology. (*A*) Transverse section of the human thalamus showing histological labeling of various thalamic nuclei adapted and modified from Mai et al. (2008) (with copyright permission from the publisher Elsevier). (*B*) The white outline (highlighted by arrows) shows the overlap between structural and functional connectivity with motor/premotor cortex. Overlap region localizes to nuclei VL, VLP. (*C*) Overlap with prefrontal cortex localizes to MD, VA, and anterior nuclei. (*D*) Overlap with temporal cortex localizes to MGN. Principal cortical targets in the legend are derived from Jones (2007). (*E*) Overlap with parietal/occipital cortex localizes to lateral pulvinar. (*F*) Overlap with somatosensory cortex localizes to anterior pulvinar.

DTI tractography defined connections between motor/premotor cortex and posterior portions of VLP, whereas functional connectivity results were more restricted to anterior and medial parts of the thalamus (Fig. 1*B*,*C*, third column). As noted above, somatosensory connectivity with nuclei VPL was observed with structural imaging but absent with functional imaging (Fig. 1*B*,*C*, fourth column). Functional correlations with somatosensory cortex were predominantly circumscribed to the anterior pulvinar (Fig. 1*B*, fourth column). A closer look at the fcMRI results in region VPL showed noticeably weak functional correlations with all cortical ROIs, although motor/premotor cortex still demonstrated statistically significant values in this region (Fig. 2).

Discussion

The high overall correspondence between the structural and functional results suggests two important implications. First, the substantial overlap between observed structure and function along with their correspondence with histology supports the feasibility and validity of the two imaging approaches in mapping thalamocortical connectivity. In the current work, measurements of structural and functional connectivity within the thalamocortical system were performed independently. This is to be contrasted with a large body of existing work where *task-evoked* fMRI is used to define a priori ROIs for use in constraining tractography results, in essence asking the binary question of whether a structural connection exists given a set of functional activation regions (see Rykhlevskaia et al. 2008) for a review of this literature). Here, the pattern of connectivity generated with one method is not influenced by the other method. It is only at the postprocessing stage that the results from both approaches are combined for comparison purposes. It should be noted that our present results extend the findings of a previous study which demonstrated the correspondence between DTI tractography and *task-evoked* fMRI in select thalamic nuclei (Johansen-Berg et al. 2005).

The second implication of the substantial overlap in observed structure and function is that a straightforward model of neuronal activity reflecting more direct physical connectivity is capable of explaining much of the mapping results. In correlation mapping of fMRI activity, it is usually an open question whether the observed correlation is a result of more direct (fewer synaptic junctions) or less direct connections (more synaptic junctions). In the present analysis, we can directly modify the relative contribution of these two parameters by using partial correlation to eliminate shared variance among the five cortical ROIs, thereby mitigating the contributions of cortico-cortical interactions in the generation of thalamic correlation maps. At a global level, the average BOLD signal across all voxels in the brain is significantly correlated with much of gray matter, including the thalamus (Fox et al. 2009). Partial correlation also eliminates globally shared signals, whether of neuronal or non-neuronal origin (Birn et al. 2006). The result of this analysis step is a delineation of neuronal activity that is reflective of more direct physical connectivity and therefore corresponds better with DTI tractography results which predominantly track long distance fiber pathways with few intervening synapses.

Interpretation of Connectivity Differences

Areas of observed differences clearly exist in the present results, suggesting a more complex interpretation. The greatest difference by voxel count is in connectivity with motor/premotor cortex (Fig. 4). There is a shift in the approximate boundary between motor/premotor regions and prefrontal regions of the thalamus, as well as a large associated shift in peak foci of localization (Fig. 4*A*,*B*). Figure 4*E* showed that this effect may be related to spatial nonuniformity of correlations with each cortical ROI. Despite the use of an anatomical parcellation scheme, the DMN emerged as the principal functional system to retain its long range functional connections. The robustness of this functional system may be related to graph theoretic descriptions of hub-like properties of some of its canonical nodes (Hagmann et al. 2008).

The functional cohesiveness of the DMN shown here suggests the distinctiveness of this functional network and also suggests the presence of polysynaptic contributions to our functional results. From a cortical parcellation perspective, these polysynaptic influences would likely be better controlled for in our partial correlation strategy if the size of our ROIs

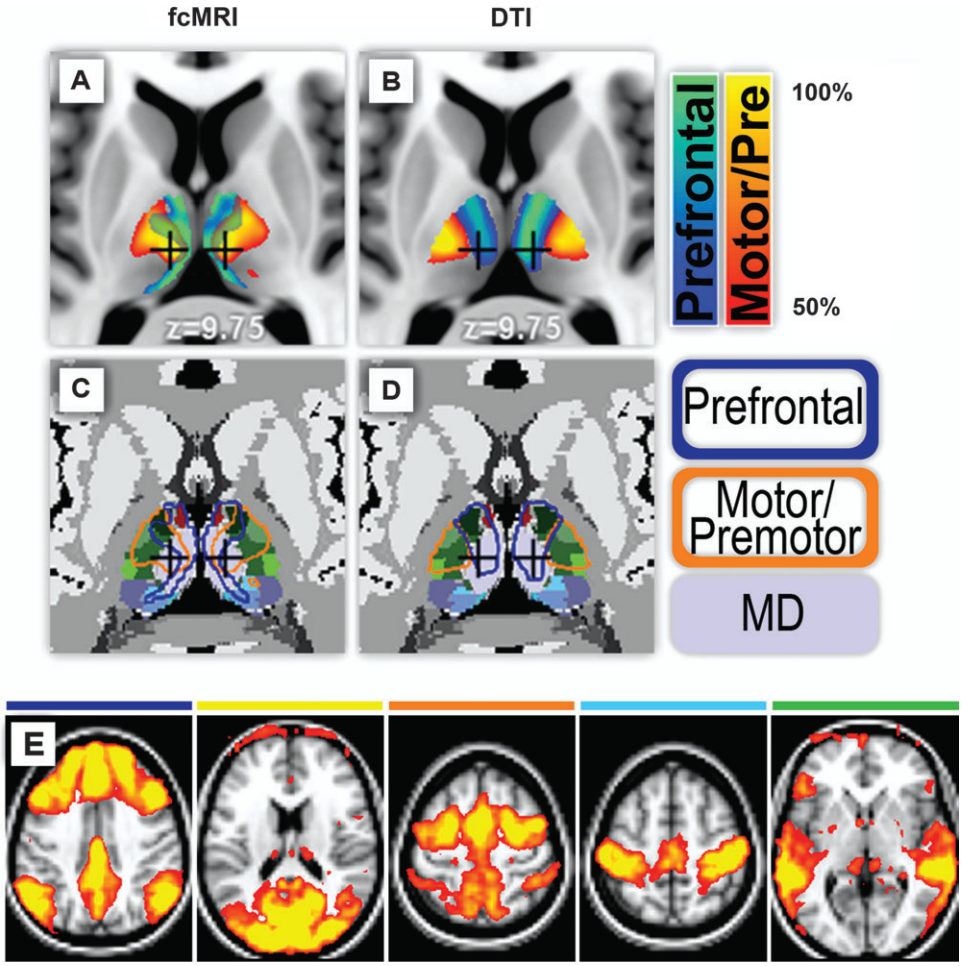

Figure 4. Differences between observed structure and function. (*A*) Motor/premotor cortex functionally correlated with thalamic nuclei VL, VLP that are traditionally known to project principally to motor/premotor cortex. However, the locus of maximal correlation was observed in a more medial thalamic area (crosshairs). (*B*) This area of the thalamus (crosshairs) exhibits the highest probabilistic DTI tractography with prefrontal cortex. (*C*,*D*) The area in question (crosshairs) histologically is the lateral extent of the MD nucleus. Functional and structural mapping results are outlined in (*C*,*D*) on top of histology (Mai et al. 2008; with copyright permission from the publisher Elsevier). (*E*) Cortical localization using same partial correlation strategy and the same cortical ROIs defined in Figure 1*A* (thresholded at *Z* score of 5–15). Most of the cortical correlations are well-restricted to within the boundary of the cortical ROI that generated the map. The major exception to this rule is cortical localization using the prefrontal ROI. In addition to high correlations with most of the prefrontal cortex, there is clear localization with the DMN.

were decreased (thus possibly increasing the correspondence between fcMRI and DTI tractography results), although we would lose whole brain coverage if the number of our ROIs were not dramatically increased (note that increasing the ROI number to double digits would not be ideal given a partial correlation strategy because of the reduction in signal to noise; see Zhang et al. 2008). Other polysynaptic interactions also likely contribute to our observations in ways that we do not control for in the present analysis. For example there are known subcortico-subcortical interactions such as those mediated by the thalamic reticular nucleus (Guillery and Harting 2003) and the brainstem reticular formation (Jones 2008). In contrast, DTI tractography results generated in the current study predominantly reflect more direct white matter pathways between the thalamus and cortex. Inference on less direct pathways such as those involving cortico-cortical connections can be performed with multi-ROI/graph theoretic measures, but the accuracy of these reconstructed polysynaptic pathways scales inversely with the number of synapses (i.e., graph nodes) involved in the pathway and the acquisition resolution. Thus, in a comparison of the two methods, one should be aware of inherent limitations in inferring functional connectivity strictly on the basis of tractography alone and vice versa. However, the limitation of each lone standing method highlights the complementary nature of the two imaging modalities. Empirically derived measures of functional connectivity can serve as a physiological constraint on the extensive permutation of possible polysynaptic anatomical connections derived from DTI tractography. Likewise, DTI tractography can often be used to generate the most plausible anatomical tract connecting two brain regions that have correlated neuronal activity (see Honey et al. 2009 for an excellent example of a graph theoretic approach to combining fcMRI and DTI tractography results).

Methodological idiosyncrasies also contribute to observed differences. In the present analysis, we utilized probabilistic tractography which is able to track through areas of the brain near gray matter (Behrens, Johansen-Berg, et al. 2003). This differs from the very limited number of studies that have combined fcMRI with diffusion weighted imaging (Koch et al. 2002; Skudlarski et al. 2008; van den Heuvel et al. 2008, 2009; Greicius et al. 2009; Honey et al. 2009), all of which have used

conventional streamline tractography which produce reliable results only in brain areas where anisotropy is high (Behrens, Johansen-Berg, et al. 2003). This distinction in tractography methodology is an important point of consideration and represents a crucial step in the feasibility of thalamocortical structural mapping (Behrens, Johansen-Berg, et al. 2003). However, even with this technical advance in the science of tractography, there are still well known and well-described current limitations (Behrens et al. 2007). The probabilistic algorithm utilized, in part, accounts for crossing fibers (Behrens et al. 2007), but areas with major fiber bundles still tend to suppress tracking of smaller fiber bundles crossing perpendicular to them. For example, the MGN can be distinguished from LGN based on differences in their connectivity profiles but showing that the connections from MGN reliably and accurately traverse to auditory cortex has been a much harder task due to crossing fibers from the optic radiations (Devlin et al. 2006; Behrens et al. 2007). In the current work, functional mapping from temporal cortex appeared to generate more specific localization to MGN than its DTI counterpart (Fig. 1*B–D*, far right panel), but the best definition of MGN from an anatomical point of view comes from the area of overlap between the two methods (Fig. 3*D*).

Methodological variability can be seen to have a pronounced effect in the winner-take-all projections (Fig. 2). Because this data reduction technique performs segmentation based only on the highest values, the boundaries of the WTA maps are expected to be more variable between the two methods and more prone to methodological idiosyncrasies. Notably, borders in DTI WTA maps are qualitatively more stripe-like, whereas fcMRI WTA borders better resemble irregular ellipsoids. This pattern is somewhat expected given that probabilistic tracts from deep thalamic nuclei have to physically pass through the outer surface of the thalamus on their way to the cortex, thus contributing to strip-like patterns. In this sense, inner and outer layers of the thalamus are less dependent on each other using functional imaging. Instead, the BOLD signal is strongest in gray matter and significantly attenuated in white matter structures.

Other Considerations

The current choice of thresholding was chosen based on a percentage of the maximum correlation/probability value to better accommodate the differences in unit measurements from the two disparate methods. One advantage of our percentage thresholding approach is that it does not artificially place a constraint on the number of voxels displayed from each method. Nevertheless, for our fcMRI results, all displayed voxels satisfied a multiple comparisons statistical significance test at $P < 0.05$ determined by a bootstrap estimation on the data (Zhang et al. 2008). We, however, performed an alternative thresholding scheme in which the *functional data* were thresholded at a multiple comparisons corrected significance of $P = 0.05$ and then the DTI data were thresholded at a level that produced an equal number of displayed voxels. This alternative strategy produced results qualitatively similar to those presented in Figure 1 (data not shown), only with less degrees of freedom in the display parameters.

Conclusions

In the current work, we have demonstrated that structural and functional mapping of the thalamocortical system, performed independently of each other, demonstrate good overall correspondence. Areas of overlap between the two methods match well with histological partitioning of the human thalamus and connectional anatomy derived from non-human primates. Within the scope of the thalamocortical system, the correspondence in functional activity with more direct anatomical connectivity reinforces the notion that the thalamus is a relay structure of the brain that faithfully performs the duty of signal transmission. More generally, fcMRI and DTI will be increasingly utilized in combined structure/function studies. In this respect, the current results provide a validation of combined imaging approaches with comparison to a histological "gold standard".

Differences between the two techniques do exist, and both results may be equally valid given the two approaches measure different aspects of "connectivity". In light of these differences, caution is warranted when inferring functional interactions strictly on the basis of DTI tractography, and vice versa. Each technique provides unique and complementary information that should be interpreted in their corresponding context. Here, we have demonstrated the feasibility of combining these two approaches within the thalamocortical system. In the larger scope, an obvious complementarity exists between fcMRI and probabilistic DTI tractography toward a global understanding of the brain's physiology, both in health and disease.

Supplementary Material

Supplementary material can be found at: http://www.cercor.oxfordjournals.org/

Funding

National Institutes of Health (NIH) (NS06833) to M.E.R.; National Institutes of Mental Health (NIMH) (F30MH083483) to D.Z.; and NIH (K23 HD053212) to J.S.S.

Notes

Conflict of Interest: None declared.

Address correspondence to Dongyang Zhang, BA, Department of Radiology, Washington University, USA. Email: zhangd@npg.wustl.edu.

References

Baird AA, Colvin MK, Vanhorn JD, Inati S, Gazzaniga MS. 2005. Functional connectivity: integrating behavioral, diffusion tensor imaging, and functional magnetic resonance imaging data sets. J Cogn Neurosci. 17:687–693.

Behrens TE, Berg HJ, Jbabdi S, Rushworth MF, Woolrich MW. 2007. Probabilistic diffusion tractography with multiple fibre orientations: what can we gain? Neuroimage. 34:144–155.

Behrens TE, Johansen-Berg H, Woolrich MW, Smith SM, Wheeler-Kingshott CA, Boulby PA, Barker GJ, Sillery EL, Sheehan K, Ciccarelli O, et al. 2003. Non-invasive mapping of connections between human thalamus and cortex using diffusion imaging. Nat Neurosci. 6:750–757.

Behrens TE, Woolrich MW, Jenkinson M, Johansen-Berg H, Nunes RG, Clare S, Matthews PM, Brady JM, Smith SM. 2003. Characterization and propagation of uncertainty in diffusion-weighted MR imaging. Magn Reson Med. 50:1077–1088.

Birn RM, Diamond JB, Smith MA, Bandettini PA. 2006. Separating respiratory-variation-related fluctuations from neuronal-activity-related fluctuations in fMRI. Neuroimage. 31:1536–1548.

Biswal B, Yetkin FZ, Haughton VM, Hyde JS. 1995. Functional connectivity in the motor cortex of resting human brain using echo-planar MRI. Magn Reson Med. 34:537–541.

Boly M, Phillips C, Tshibanda L, Vanhaudenhuyse A, Schabus M, Dang-Vu TT, Moonen G, Hustinx R, Maquet P, Laureys S. 2008. Intrinsic brain activity in altered states of consciousness: how conscious is the default mode of brain function? Ann N Y Acad Sci. 1129:119–129.

Cordes D, Haughton VM, Arfanakis K, Wendt GJ, Turski PA, Moritz CH, Quigley MA, Meyerand ME. 2000. Mapping functionally related regions of brain with functional connectivity MR imaging. Am J Neuroradiol. 21:1636–1644.

Devlin JT, Sillery EL, Hall DA, Hobden P, Behrens TE, Nunes RG, Clare S, Matthews PM, Moore DR, Johansen-Berg H. 2006. Reliable identification of the auditory thalamus using multi-modal structural analyses. Neuroimage. 30:1112–1120.

Fox MD, Raichle ME. 2007. Spontaneous fluctuations in brain activity observed with functional magnetic resonance imaging. Nat Rev Neurosci. 8:700–711.

Fox MD, Snyder AZ, Vincent JL, Corbetta M, Van Essen DC, Raichle ME. 2005. The human brain is intrinsically organized into dynamic, anticorrelated functional networks. Proc Natl Acad Sci USA. 102:9673–9678.

Fox MD, Snyder AZ, Vincent JL, Raichle ME. 2007. Intrinsic fluctuations within cortical systems account for intertrial variability in human behavior. Neuron. 56:171–184.

Fox MD, Zhang D, Snyder AZ, Raichle ME. 2009. The global signal and observed anticorrelated resting state brain networks. J Neurophysiol. 101:3270–3283.

Greicius MD, Krasnow B, Reiss AL, Menon V. 2003. Functional connectivity in the resting brain: a network analysis of the default mode hypothesis. Proc Natl Acad Sci USA. 100:253–258.

Greicius MD, Supekar K, Menon V, Dougherty RF. 2009. Resting-state functional connectivity reflects structural connectivity in the default mode network. Cereb Cortex. 19:72–78.

Guillery RW, Harting JK. 2003. Structure and connections of the thalamic reticular nucleus: advancing views over half a century. J Comp Neurol. 463:360–371.

Hagmann P, Cammoun L, Gigandet X, Meuli R, Honey CJ, Wedeen VJ, Sporns O. 2008. Mapping the structural core of human cerebral cortex. PLoS Biol. 6:e159.

Honey CJ, Sporns O, Cammoun L, Gigandet X, Thiran JP, Meuli R, Hagmann P. 2009. Predicting human resting-state functional connectivity from structural connectivity. Proc Natl Acad Sci USA. 106:2035–2040.

Horovitz SG, Fukunaga M, de Zwart JA, van Gelderen P, Fulton SC, Balkin TJ, Duyn JH. 2008. Low frequency BOLD fluctuations during resting wakefulness and light sleep: a simultaneous EEG-fMRI study. Hum Brain Mapp. 29:671–682.

Jenkins GM, Watts DG. 1968. Spectral analysis and its applications. Oakland (CA): Holden-Day.

Jenkinson M, Smith S. 2001. A global optimisation method for robust affine registration of brain images. Med Image Anal. 5:143–156.

Johansen-Berg H, Behrens TE, Sillery E, Ciccarelli O, Thompson AJ, Smith SM, Matthews PM. 2005. Functional-anatomical validation and individual variation of diffusion tractography-based segmentation of the human thalamus. Cereb Cortex. 15:31–39.

Johnston JM, Vaishnavi SN, Smyth MD, Zhang D, He BJ, Zempel JM, Shimony JS, Snyder AZ, Raichle ME. 2008. Loss of resting interhemispheric functional connectivity after complete section of the corpus callosum. J Neurosci. 28:6453–6458.

Jones DK. 2008. Tractography gone wild: probabilistic fibre tracking using the wild bootstrap with diffusion tensor MRI. IEEE Trans Med Imaging. 27:1268–1274.

Jones EG. 2007. The thalamus. Cambridge, UK: Cambridge University Press.

Koch MA, Norris DG, Hund-Georgiadis M. 2002. An investigation of functional and anatomical connectivity using magnetic resonance imaging. Neuroimage. 16:241–250.

Lancaster JL, Glass TG, Lankipalli BR, Downs H, Mayberg H, Fox PT. 1995. A modality-independent approach to spatial normalization of tomographic images of the human brain. Hum Brain Mapp. 3:209–223.

Larson-Prior LJ, Zempel JM, Nolan TS, Prior FW, Snyder AZ, Raichle ME. 2009. Cortical network functional connectivity in the descent to sleep. Proc Natl Acad Sci USA. 106:4489–4494.

Lowe MJ, Mock BJ, Sorenson JA. 1998. Functional connectivity in single and multislice echoplanar imaging using resting-state fluctuations. Neuroimage. 7:119–132.

Mai JK, Paxinos G, Voss T. 2008. Atlas of the human brain. New York: Academic Press.

Ojemann JG, Akbudak E, Snyder AZ, McKinstry RC, Raichle ME, Conturo TE. 1997. Anatomic localization and quantitative analysis of gradient refocused echo-planar fMRI susceptibility artifacts. NeuroImage. 6:156–167.

Raichle ME, Mintun MA. 2006. Brain work and brain imaging. Annu Rev Neurosci. 29:449–476.

Ray JP, Price JL. 1993. The organization of projections from the mediodorsal nucleus of the thalamus to orbital and medial prefrontal cortex in macaque monkeys. J Comp Neurol. 337:1–31.

Rowland DJ, Garbow JR, Laforest R, Snyder AZ. 2005. Registration of [18F]FDG microPET and small-animal MRI. Nucl Med Biol. 32:567–572.

Rykhlevskaia E, Gratton G, Fabiani M. 2008. Combining structural and functional neuroimaging data for studying brain connectivity: a review. Psychophysiology. 45:173–187.

Sherman SM, Guillery RW. 2006. Exploring the thalamus and its role in cortical function. Cambridge (MA): MIT Press.

Shimony JS, Burton H, Epstein AA, McLaren DG, Sun SW, Snyder AZ. 2006. Diffusion tensor imaging reveals white matter reorganization in early blind humans. Cereb Cortex. 16:1653–1661.

Skudlarski P, Jagannathan K, Calhoun VD, Hampson M, Skudlarska BA, Pearlson G. 2008. Measuring brain connectivity: diffusion tensor imaging validates resting state temporal correlations. Neuroimage. 43:554–561.

Smith SM, Jenkinson M, Woolrich MW, Beckmann CF, Behrens TE, Johansen-Berg H, Bannister PR, De Luca M, Drobnjak I, Flitney DE, et al. 2004. Advances in functional and structural MR image analysis and implementation as FSL. Neuroimage. 23(Suppl. 1):S208–S219.

Talairach J, Tournoux P. 1988. Co-planar stereotaxic atlas of the human brain; 3-dimensional proportional system: an approach to cerebral imaging. Stuttgart, New York: Georg Thieme Verlag, Thieme Medical Publishers, Inc.

Toosy AT, Ciccarelli O, Parker GJ, Wheeler-Kingshott CA, Miller DH, Thompson AJ. 2004. Characterizing function-structure relationships in the human visual system with functional MRI and diffusion tensor imaging. Neuroimage. 21:1452–1463.

van den Heuvel MP, Mandl RC, Kahn RS, Hulshoff Pol HE. 2009. Functionally linked resting-state networks reflect the underlying structural connectivity architecture of the human brain. Hum Brain Mapp. Epub ahead of print February 23, doi 10.1002/hbm.20737.

van den Heuvel M, Mandl R, Luigjes J, Hulshoff Pol H. 2008. Microstructural organization of the cingulum tract and the level of default mode functional connectivity. J Neurosci. 28:10844–10851.

Van Essen DC. 2005. A population-average, landmark- and surface-based (PALS) atlas of the human cerebral cortex. Neuroimage. 28:635–662.

Van Essen DC, Drury HA. 1997. Structural and functional analyses of human cerebral cortex using a surface-based atlas. J Neurosci. 17:7079–7102.

Van Essen DC, Drury HA, Dickson J, Harwell J, Hanlon D, Anderson CH. 2001. An integrated software suite for surface-based analyses of cerebral cortex. J Am Med Inform Assoc. 8:443–459.

Van Horn SC, Erisir A, Sherman SM. 2000. Relative distribution of synapses in the A-laminae of the lateral geniculate nucleus of the cat. J Comp Neurol. 416:509–520.

Vincent JL, Patel GH, Fox MD, Snyder AZ, Baker JT, Van Essen DC, Zempel JM, Snyder LH, Corbetta M, Raichle ME. 2007. Intrinsic functional architecture in the anesthetized monkey brain. Nature. 447:83–86.

Weatherburn CE. 1949. First course mathematical statistics. Cambridge, UK: Cambridge University Press.

Woods RP, Grafton ST, Holmes CJ, Cherry SR, Mazziotta JC. 1998. Automated image registration: I. General methods and intrasubject, intramodality validation. J Comput Assist Tomogr. 22:139–152.

Woolrich MW, Jbabdi S, Patenaude B, Chappell M, Makni S, Behrens T, Beckmann C, Jenkinson M, Smith SM. 2009. Bayesian analysis of neuroimaging data in FSL. Neuroimage. 45:S173–S186.

Zhang D, Snyder AZ, Fox MD, Sansbury MW, Shimony JS, Raichle ME. 2008. Intrinsic functional relations between human cerebral cortex and thalamus. J Neurophysiol. 100:1740–1748.